Research Article

Mathematical Methods in the Applied Sciences

Received 19 November 2015

Published online 19 July 2016 in Wiley Online Library

(wileyonlinelibrary.com) DOI: 10.1002/mma.4093
MOS subject classification: 65M06; 35K55

Practical estimation of a splitting parameter for a spectral method for the ternary Cahn–Hilliard system with a logarithmic free energy

Darae Jeong and Junseok Kim[*†]

Communicated by W. Wendland

We propose a practical estimation of a splitting parameter for a spectral method for the ternary Cahn–Hilliard system with a logarithmic free energy. We use Eyre's convex splitting scheme for the time discretization and a Fourier spectral method for the space variables. Given an absolute temperature, we find composition values that make the total free energy be minimum. Then, we find the splitting parameter value that makes the two split homogeneous free energies be convex on the neighborhood of the local minimum concentrations. For general use, we also propose a sixth-order polynomial approximation of the minimum concentration and derive a useful formula for the practical estimation of the splitting parameter in terms of the absolute temperature. The numerical tests are phase separation and total energy decrease with different temperature values. The linear stability analysis shows a good agreement between the exact and numerical solutions with an optimal value *s*. Various computational experiments confirm that the proposed splitting parameter estimation gives stable numerical results. Copyright © 2016 John Wiley & Sons, Ltd.

Keywords: ternary Cahn–Hilliard system; logarithmic free energy; spectral method; phase separation; optimal splitting parameter

1. Introduction

In this paper, we propose a practical estimation of a splitting parameter for a spectral method for the ternary Cahn–Hilliard (CH) system with a logarithmic free energy. For $i = 1, 2, 3$, let $c_i = c_i(\mathbf{x}, t)$ be the i-th concentration of the ternary mixture. Then, the ternary CH system with a logarithmic free energy is as follows [1]:

$$\frac{\partial c_1}{\partial t} = \Delta \mu_1, \ \mathbf{x} \in \Omega, \ t > 0, \tag{1}$$

$$\mu_1 = \theta \ln(c_1) - \theta_c c_1 - \epsilon^2 \Delta c_1 - \frac{\theta}{3} \ln(c_1 c_2 c_3), \tag{2}$$

$$\frac{\partial c_2}{\partial t} = \Delta \mu_2, \tag{3}$$

$$\mu_2 = \theta \ln(c_2) - \theta_c c_2 - \epsilon^2 \Delta c_2 - \frac{\theta}{3} \ln(c_1 c_2 c_3), \tag{4}$$

$$\frac{\partial c_3}{\partial t} = \Delta \mu_3, \tag{5}$$

$$\mu_3 = \theta \ln(c_3) - \theta_c c_3 - \epsilon^2 \Delta c_3 - \frac{\theta}{3} \ln(c_1 c_2 c_3), \tag{6}$$

Department of Mathematics, Korea University, Seoul 136-713, Korea
** Correspondence to: Junseok Kim, Department of Mathematics, Korea University, Seoul 136-713, Korea.*
† E-mail: cfdkim@korea.ac.kr

where Ω is an open domain in $\mathbb{R}^d$ $(d = 1, 2)$, θ is the absolute temperature, θ_c is the critical temperature, and ϵ is the gradient energy coefficient. Here, θ, θ_c, and ϵ are positive constants with $\theta < \theta_c$. We use the periodic boundary conditions for the system. The ternary CH system (1)–(6) can be derived from the following energy functional [2]:

$$\mathcal{E}(t) = \int_\Omega \left(F(c_1, c_2, c_3) + \sum_{i=1}^{3} \frac{\epsilon^2}{2} |\nabla c_i|^2 \right) d\mathbf{x},$$

where $F(c_1, c_2, c_3)$ is the free energy density of a homogeneous system with concentration c_1, c_2, and c_3 as

$$F(c_1, c_2, c_3) = \theta(c_1 \ln c_1 + c_2 \ln c_2 + c_3 \ln c_3) + \theta_c(c_1c_2 + c_2c_3 + c_3c_1). \tag{7}$$

Generalization of the binary CH equation [3] appears first with deFontaine [4–6] and with Morral and Cahn [7]. The ternary CH system was applied to the prediction of microstructural evolutions in Fe–Cr–Mo ternary alloys in [8, 9]. The authors in [10] studied the effect of Mo on the microstructure evolution, and coarsening kinetics of γ' precipitates in the Ni–Al–Mo system is studied using phase-field simulations. Using a phase-field method, the phase transformation process and morphological change of microstructure were theoretically simulated for Fe–Al–Co ternary ordering alloy systems [11]. The microstructure simulation of spinodal decomposition was carried out in the isothermally aged Cu-46 at.%Ni-4 at.%Fe alloys using the phase-field method [12].

The main purpose of this work is to propose an estimation of a splitting parameter for the ternary CH system with a thermodynamically consistent logarithmic free energy for a three-component mixture.

The contents of this paper are as follows. In Section 2, we consider a Fourier spectral method for the ternary CH system. In Section 3, various computational experiments such as phase separation, total energy decrease with different temperature values, and linear stability analysis are performed, which confirm that the proposed splitting parameter estimation gives stable numerical results. Finally, conclusions are drawn in Section 4.

2. Numerical solution

For simplicity of exposition, we consider the numerical solution in one-dimensional space, $\Omega = [a, b]$. Extension to the other higher-dimensional problems are straightforward.

Let N_x be a positive even integer, $h = (b - a)/N_x$ be the uniform mesh size, $\Omega_h = \{x_m | x_m = a + mh,\ 0 \le m \le N_x\}$ be the set of grid points, and Δt be the time step. Figure 1 illustrates the spatial grid. Let $\phi = c_1$, $\mu = \mu_1$, $\psi = c_2$, and $\nu = \mu_2$. Let ϕ_m^k be approximation of $\phi(x_m, k\Delta t)$. Here, k means the time level. The others, ψ_m^k, μ_m^k, and ν_m^k, are similarly defined. In this paper, we consider a Fourier spectral method and propose practical splitting parameter estimation for Eqs (1)–(4):

$$\frac{\phi_m^{k+1} - \phi_m^k}{\Delta t} = \Delta \mu_m^{k+1}, \tag{8}$$

$$\begin{aligned} \mu_m^{k+1} = {} & \theta \ln\left(\phi_m^k\right) - (s+1)\theta_c \phi_m^k + s\theta_c \phi_m^{k+1} - \epsilon^2 \Delta \phi_m^{k+1} \\ & - \frac{\theta}{3} \ln\left[\left(\phi_m^k \psi_m^k (1 - \phi_m^k - \psi_m^k)\right)\right], \end{aligned} \tag{9}$$

$$\frac{\psi_m^{k+1} - \psi_m^k}{\Delta t} = \Delta \nu_m^{k+1}, \tag{10}$$

$$\begin{aligned} \nu_m^{k+1} = {} & \theta \ln\left(\psi_m^k\right) - (s+1)\theta_c \psi_m^k + s\theta_c \psi_m^{k+1} - \epsilon^2 \Delta \psi_m^{k+1} \\ & - \frac{\theta}{3} \ln\left[\left(\phi_m^k \psi_m^k (1 - \phi_m^k - \psi_m^k)\right)\right], \end{aligned} \tag{11}$$

where s is a positive number. Here, we only solve the equations with ϕ and ψ because the third concentration can be defined as $1 - \phi - \psi$.

2.1. Fourier spectral method

For the given data $\{\phi_1^k, \phi_2^k, \cdots, \phi_{N_x}^k\}$, the discrete Fourier transform is defined as

$$\hat{\phi}_p^k = \sum_{m=1}^{N_x} \phi_m^k e^{-i\xi_p x_m},$$

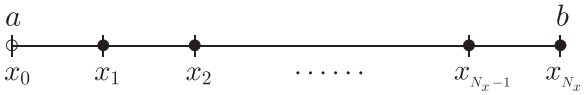

Figure 1. Uniform grid $\{x_0, x_1, \cdots, x_{N_x}\}$ with $h = x_{m+1} - x_m$ for $m = 0, \cdots, N_x - 1$.

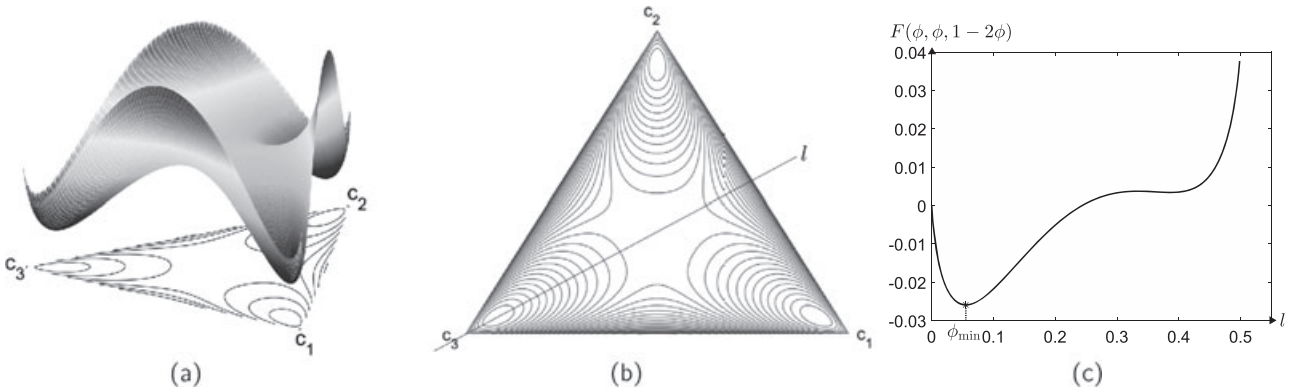

Figure 2. (a) Free energy surface $F(c_1, c_2, c_3)$, (b) its contour plot, and (c) free energy $F(\phi, \phi, 1-2\phi)$ and $\phi_{\min}$ on line l.

where $\xi_p = 2p\pi/(b-a)$. The inverse discrete Fourier transform is

$$\phi_m^k = \frac{1}{N_x} \sum_{p=-N_x/2}^{N_x/2-1} \hat{\phi}_p^k e^{i\xi_p x_m}. \tag{12}$$

Let us assume that

$$\phi(x, k\Delta t) = \frac{1}{N_x} \sum_{p=-N_x/2}^{N_x/2-1} \hat{\phi}_p^k e^{i\xi_p x}. \tag{13}$$

Then, the second-order and fourth-order partial derivatives are given as

$$\Delta\phi(x, k\Delta t) = -\frac{1}{N_x} \sum_{p=-N_x/2}^{N_x/2-1} \xi_p^2 \hat{\phi}_p^k e^{i\xi_p x}, \tag{14}$$

$$\Delta^2\phi(x, k\Delta t) = \frac{1}{N_x} \sum_{p=-N_x/2}^{N_x/2-1} \xi_p^4 \hat{\phi}_p^k e^{i\xi_p x}. \tag{15}$$

By substituting Eqs (13)–(15) into Eqs (8) and (9), we have

$$\frac{\hat{\phi}_p^{k+1} - \hat{\phi}_p^k}{\Delta t} = -\xi_p^2 \hat{f}_p^k - \xi_p^2 s\theta_c \hat{\phi}_p^{k+1} - \xi_p^4 \epsilon^2 \hat{\phi}_p^{k+1}.$$

Here, $\hat{f}_p^k = \sum_{m=1}^{N_x} f_m^k e^{-i\xi_p x_m}$, where $f_m^k = \theta \ln(\phi_m^k) - (s+1)\theta_c \phi_m^k - \theta \ln\left[\left(\phi_m^k \psi_m^k (1 - \phi_m^k - \psi_m^k)\right]/3$. Then, we have

$$\hat{\phi}_p^{k+1} = \left(\hat{\phi}_p^k/\Delta t - \xi_p^2 \hat{f}_p^k\right) / \left(1/\Delta t + \xi_p^2 s\theta_c + \xi_p^4 \epsilon^2\right). \tag{16}$$

Finally, using Eqs (12) and (16), we obtain $(k+1)$-th time step solution, ϕ_m^{k+1} for $m = 1, \cdots, N_x$. Similarly, we can obtain ψ_m^{k+1}.

2.2. *Optimal splitting factor s**

By Eyre's theorem [13, 14], if we can split the free energy appropriately into contractive and expansive parts and then treat the contractive part implicitly and the expansive part explicitly, the numerical splitting algorithm is unconditionally gradient stable. In the right-hand side of Eq. (9), $\theta \ln(\phi^k) - (s+1)\theta_c \phi^k + s\theta_c \phi^{k+1}$ can be rewritten as $F_c'(\phi^{k+1}) - F_e'(\phi^k)$, where $F_c(\phi) = 0.5 s\theta_c \phi^2$ is a contractive term and $F_e(\phi) = 0.5(s+1)\theta_c \phi^2 - \theta\phi \ln(\phi) + \theta\phi$ is an expansive term. Note that both functions $F_c(\phi)$ and $F_e(\phi)$ are strictly convex in the region satisfying $s > 0$, $\theta_c > 0$, and

$$\left\{\phi \in (0,1) : F_e''(\phi) = (s+1)\theta_c - \frac{\theta}{\phi} > 0\right\}. \tag{17}$$

To find the optimal splitting factor, we use the minimum point $\phi_{\min}$ as the minimum point at which $F(\phi, \phi, 1-2\phi)$ achieves a minimum; see Eq. (7) for the definition of F. Figure 2 represents the free energy surface $F(c_1, c_2, c_3)$ and its contour plot. As shown in Figure 3, the free energy has three local minima. By Cahn–Hilliard dynamics, each c_i moves the position of the local minima to minimize the energy. To minimize the local discretization error [13], we need to take the value of s as small as possible. At the same time, we want to keep the strictly convexity of $F_e(\phi)$, that is, Eq. (17). Therefore, in the proposed method, we compute the minimum point $\phi_{\min}$, and based on the value, we define the splitting parameter s.

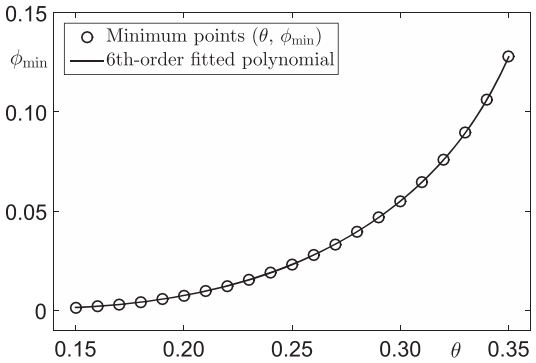

Figure 3. Minimum points $\phi_{\min}$ (circled symbol) with respect to θ and a sixth-order best-fitted polynomial (solid line) when $\theta_c = 1$.

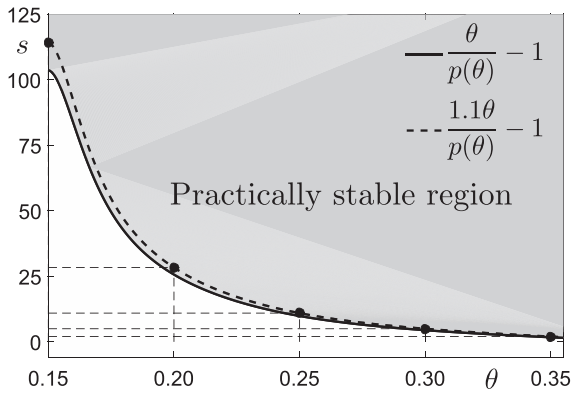

Figure 4. Practically stable region of s over θ when $\theta_c = 1$. The dashed line denotes optimal splitting factor s^* against θ.

Let $g(\phi) = F(\phi, \phi, 1-2\phi)$, then

$$g'(\phi_{\min}) = 2\theta \ln\left(\frac{\phi_{\min}}{1-2\phi_{\min}}\right) + \theta_c(2 - 6\phi_{\min}) = 0. \tag{18}$$

We numerically solve Eq. (18) by using **fzero** command in MATLAB [15]. Figure 3 shows the minimum points $\phi_{\min}$ (circled symbol) with respect to θ and a sixth-order best-fitted polynomial (solid line) when $\theta_c = 1$. Here, using **polyfit** command in MATLAB, we find the polynomial of order 6 that fits best to the given data points $(\theta, \phi_{\min})$ as

$$\begin{aligned} p(\theta) = {} & 9420.12298\,\theta^6 - 13037.1741\,\theta^5 + 7460.65877\,\theta^4 \\ & - 2249.07797\,\theta^3 + 377.41886\,\theta^2 - 33.41158\,\theta + 1.21763, \end{aligned} \tag{19}$$

for $0.15 \le \theta \le 0.35$. For the reader unfamiliar with MATLAB, we provide the code in the Appendix.

Now, by the condition (17) and approximated polynomial (19), we obtain the condition of splitting factor s satisfying convexity of $F_e(\phi)$ as

$$s > \frac{\theta}{\phi_{\min}\theta_c} - 1 \approx \frac{\theta}{p(\theta)\theta_c} - 1. \tag{20}$$

In Figure 4, practically stable region is shown in the phase plane of temperature θ and splitting parameter s using inequality Eq. (20). We define an optimal splitting factor s^* as $s^* = 1.1\theta/(\theta_c\phi_{\min}) - 1$, where 1.1 is a safety factor. Therefore, for a given temperature θ, we can automatically decide the splitting factor s. For example, when $\theta_c = 1$, the optimal splitting factor s^* is

$$s^* = 1.1\theta/p(\theta) - 1.$$

In Figure 4, we can also see $\theta/(\theta_c\phi_{\min}) - 1$ and $1.1\theta/(\theta_c\phi_{\min}) - 1$ with solid and dashed lines, respectively. We note that the author in [16] suggested choosing optimal values of splitting parameter as a future research.

Note that our strategy for the optimal splitting parameter is based on the assumption $\phi \ge \phi_{\min}$. In fact, there is no maximal principle in the ternary CH equation. However, the minimum values of the phase stay in the neighborhood of $\phi_{\min}$ during evolution. Even though we derive the convex condition with the assumption $\phi \ge \phi_{\min}$, effective assumption is that $\phi \ge \phi_{\min}/1.1$ because of the safety factor.

3. Numerical experiments

In this section, we present various computational experiments to demonstrate that the proposed splitting parameter estimation gives stable numerical results. The numerical tests are spinodal decomposition and total energy decrease with different temperature values.

3.1. *One-dimensional space*

First, we study phase separation dynamics on one-dimensional space $\Omega = (0, 2)$ with different θ. In this numerical test, we use $N_x = 200$, $h = 0.01$, $\Delta t = 0.1$, and $\epsilon = h$. The initial conditions are set to

$$\phi(x, 0) = 0.25 + 0.1\text{rand}(x), \qquad \psi(x, 0) = 0.25 + 0.1\text{rand}(x), \tag{21}$$

where rand(x) is a random number generated uniformly in interval $[-1, 1]$. Figure 5 represents the temporal evolution of numerical solutions in the ternary system with $\theta = 0.15, 0.225$, and 0.3. The times are shown at the bottom of each figure. In early times, we can observe two phases; one of them is dominated by $1 - \phi - \psi$, and the other phase is dominated by $\phi \approx \psi$. Then, we can see three dominating phases at later times. Moreover, as the absolute temperature value θ increases, maximum concentration value decreases. With increasing absolute temperature values, we have decreasing maximum concentration values.

We define a discrete energy functional as

$$\mathcal{E}^h(\phi^k, \psi^k) = h \sum_{m=1}^{N_x} \Big(\theta \left[\phi_m^k \ln \phi_m^k + \psi_m^k \ln \psi_m^k + \left(1 - \phi_m^k - \psi_m^k\right) \ln \left(1 - \phi_m^k - \psi_m^k\right) \right] + \theta_c \left[\phi_m^k \psi_m^k + \left(\phi_m^k + \psi_m^k\right) \left(1 - \phi_m^k - \psi_m^k\right) \right] + \frac{\epsilon^2}{2} \left(\left|\nabla \phi_m^k\right|^2 + \left|\nabla \psi_m^k\right|^2 + \left|\nabla \phi_m^k + \nabla \psi_m^k\right|^2 \right) \Big),$$

where

$$\nabla \phi_m^k = \frac{1}{N_x} \sum_{p=-N_x/2}^{N_x/2-1} i \xi_p \hat{\phi}_p^k e^{i \xi_p x_m}.$$

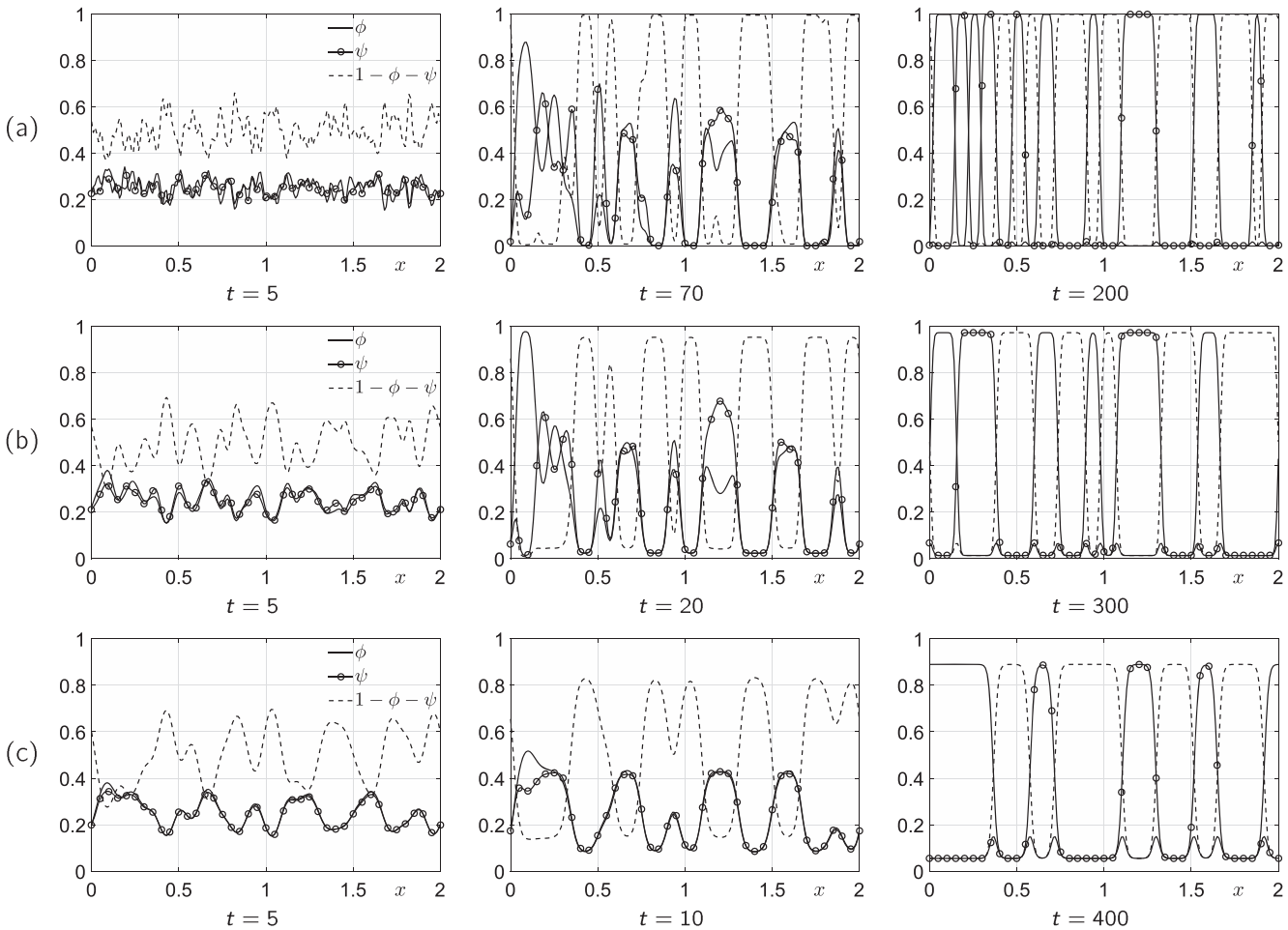

Figure 5. Numerical solutions of the ternary system with (a) $\theta = 0.15$, (b) $\theta = 0.225$, and (c) $\theta = 0.3$. The times are shown at the bottom of each figure.

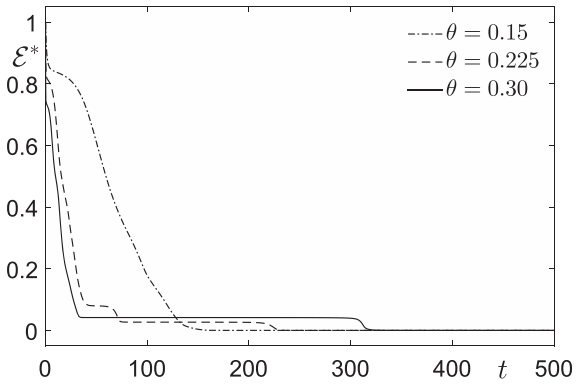

Figure 6. Scaled discrete energies $\mathcal{E}^*(\phi^k, \psi^k)$ of the numerical solutions on a ternary system with $\theta = 0.15$, 0.225, and 0.3. Here, we use the initial conditions (21).

By Eq. (22), we calculate the temporal evolutions of the discrete energy $\mathcal{E}^h(\phi^k, \psi^k)$ with $\theta = 0.15$, 0.225, and 0.3. For comparison, we define the scaled energy as

$$\mathcal{E}^*(\phi^k, \psi^k) = \frac{\mathcal{E}^h(\phi^k, \psi^k) - \mathcal{E}^h(\phi^{N_t}, \psi^{N_t})}{\mathcal{E}^h(\phi^0, \psi^0) - \mathcal{E}^h(\phi^{N_t}, \psi^{N_t})}. \tag{22}$$

These results are shown in Figure 6. In all cases, the scaled energy $\mathcal{E}^*(\phi^k, \psi^k)$ decreases as time goes on.

Next, we consider three equal concentrations as the initial condition:

$$\phi(x, 0) = 1/3 + 0.1\text{rand}(x), \qquad \psi(x, 0) = 1/3 + 0.1\text{rand}(x).$$

The other parameters are set to the same values used in the previous numerical test. Figure 7 represents the temporal evolutions of the numerical solutions of the ternary system with $\theta = 0.15$, 0.225, and 0.3. The times are shown at the bottom of each figure. We can see three phases in the early stages of phase separation. Figure 8 shows the temporal evolutions of the scaled discrete energy $\mathcal{E}^*(\phi^k, \psi^k)$ with $\theta = 0.15$, 0.225, and 0.3. They are decreasing as we expected.

3.2. *Two-dimensional space*

In this section, we present the computational results of spinodal decomposition in ternary systems on two-dimensional space. The simulations are performed on domain $\Omega = [0, 2] \times [0, 2]$ using $N_x \times N_y = 200 \times 200$ grid points with $h = 0.01$, $\Delta t = 0.1$, and $\epsilon = h$. Figure 9 represents the temporal evolution of the numerical solutions in the ternary system with the initial conditions:

$$\phi(x, y, 0) = 0.25 + 0.05\text{rand}(x, y),\ \psi(x, y, 0) = 0.25 + 0.05\text{rand}(x, y),$$

where rand(x, y) is the random value in $[-1, 1]$. To verify the stability of the numerical solution with respect to the given temperature, we perform the numerical simulations with $\theta = 0.15$, 0.225, and 0.3. By using the proposed optimal splitting factor s^*, we obtain the stable spinodal decomposition dynamics. Note that we have binary-like phase separation in early times.

In two-dimensional space, we also define a discrete energy functional as follows:

$$\begin{aligned}\mathcal{E}^h(\phi^k, \psi^k) = h^2 \sum_{n=1}^{N_y} \sum_{m=1}^{N_x} \Big(&\theta \left[\phi_{mn}^k \ln \phi_{mn}^k + \psi_{mn}^k \ln \psi_{mn}^k + \left(1 - \phi_{mn}^k - \psi_{mn}^k\right) \ln \left(1 - \phi_{mn}^k - \psi_{mn}^k\right)\right] \\ &+\theta_c \left[\phi_{mn}^k \psi_{mn}^k + \left(\phi_{mn}^k + \psi_{mn}^k\right)\left(1 - \phi_{mn}^k - \psi_{mn}^k\right)\right] + \frac{\epsilon^2}{2}\left(\left|\nabla \phi_{mn}^k\right|^2 + \left|\nabla \psi_{mn}^k\right|^2 + \left|\nabla \phi_{mn}^k + \nabla \psi_{mn}^k\right|^2\right)\Big),\end{aligned}$$

where $|\nabla \phi_{mn}^k|^2 = \left(\nabla_x \phi_{mn}^k\right)^2 + \left(\nabla_y \phi_{mn}^k\right)^2$. Here,

$$\nabla_x \phi_{mn}^k = \frac{1}{N_x N_y} \sum_{q=-N_y/2}^{N_y/2-1} \sum_{p=-N_x/2}^{N_x/2-1} i\xi_p \hat{\phi}_{pq}^k e^{i(\xi_p x_m + \zeta_q y_n)},$$

$$\nabla_y \phi_{mn}^k = \frac{1}{N_x N_y} \sum_{q=-N_y/2}^{N_y/2-1} \sum_{p=-N_x/2}^{N_x/2-1} i\zeta_q \hat{\phi}_{pq}^k e^{i(\xi_p x_m + \zeta_q y_n)}.$$

Figure 10 shows the scaled energy (22) with $\theta = 0.15$, 0.0225, and 0.3. In all cases, we see that the scaled energy $\mathcal{E}^*$ is decreasing as time goes on.

We present the second simulation on two-dimensional space with the initial condition as

$$\phi(x, y, 0) = 1/3 + 0.05\text{rand}(x, y),\ \psi(x, y, 0) = 1/3 + 0.05\text{rand}(x, y).$$

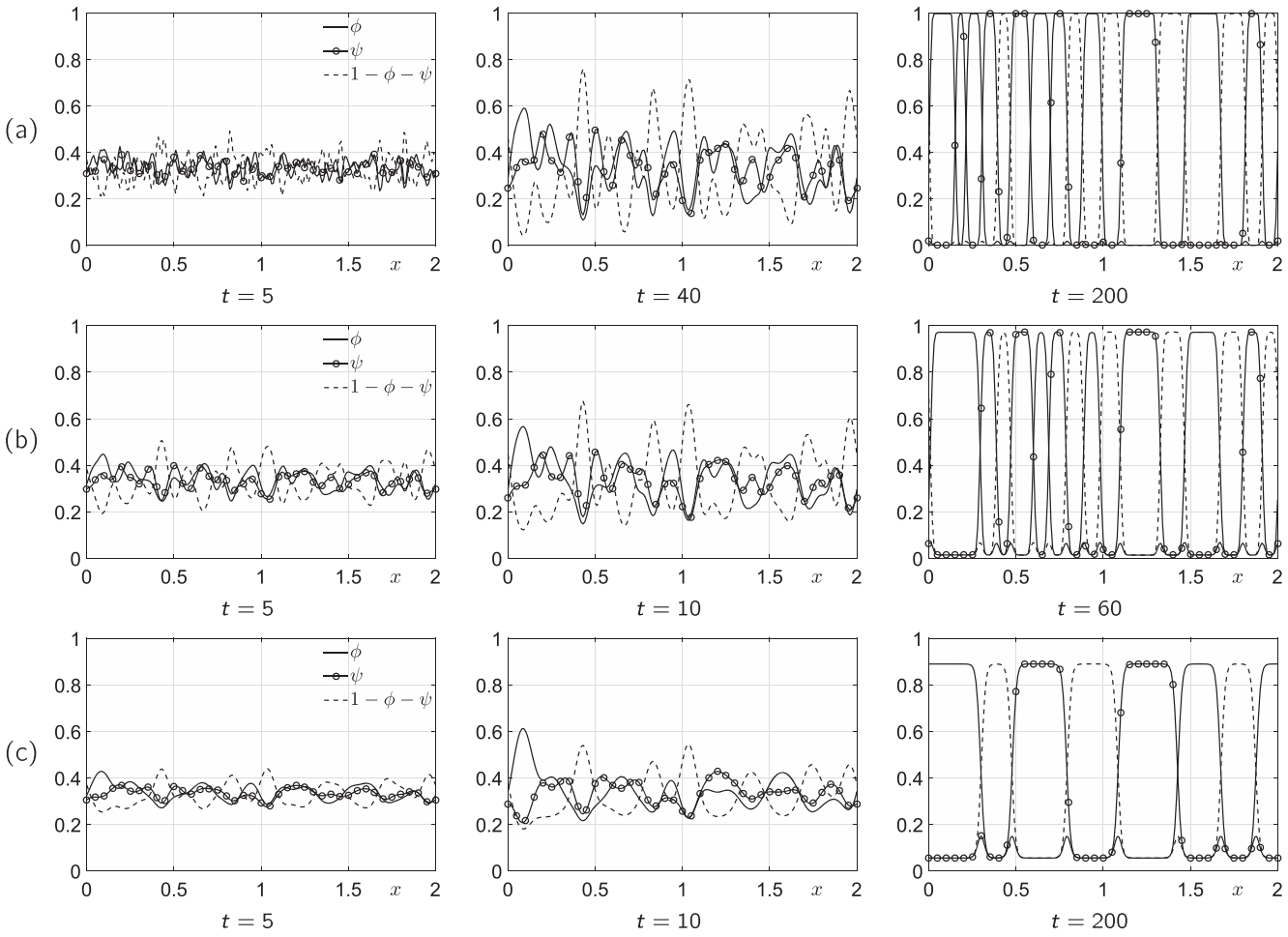

Figure 7. Numerical solution of a ternary system with (a) $\theta = 0.15$, (b) $\theta = 0.225$, and (c) $\theta = 0.3$. The times are shown at the bottom of each figure.

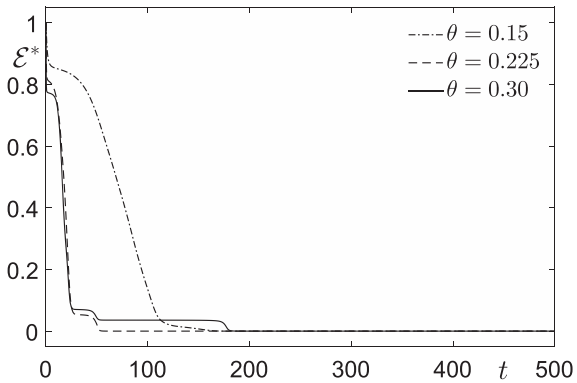

Figure 8. Scaled discrete energies $\mathcal{E}^*(\phi^k, \psi^k)$ of the numerical solutions on the ternary system with $\theta = 0.15$, 0.225, and 0.3.

As shown in Figure 11, we can see the phase separation of three phases from the early stages.

Figure 12 shows the scaled discrete energy of numerical solution in a ternary system. As we expected, the energies decreases as time goes on.

3.3. *Effect of splitting parameter s*

In this section, we show the effect of splitting parameter s. To show the effect, we perform a linear stability analysis. With the mean concentration as $\mathbf{m} = (m, m, 1-2m)$, we will find a solution having the following form

$$\begin{pmatrix} \phi(x,t) \\ \psi(x,t) \end{pmatrix} = \begin{pmatrix} m \\ m \end{pmatrix} + \sum_{k=1}^{\infty} \begin{pmatrix} \alpha_k(t)\cos(k\pi x) \\ \beta_k(t)\cos(k\pi x) \end{pmatrix}, \tag{23}$$

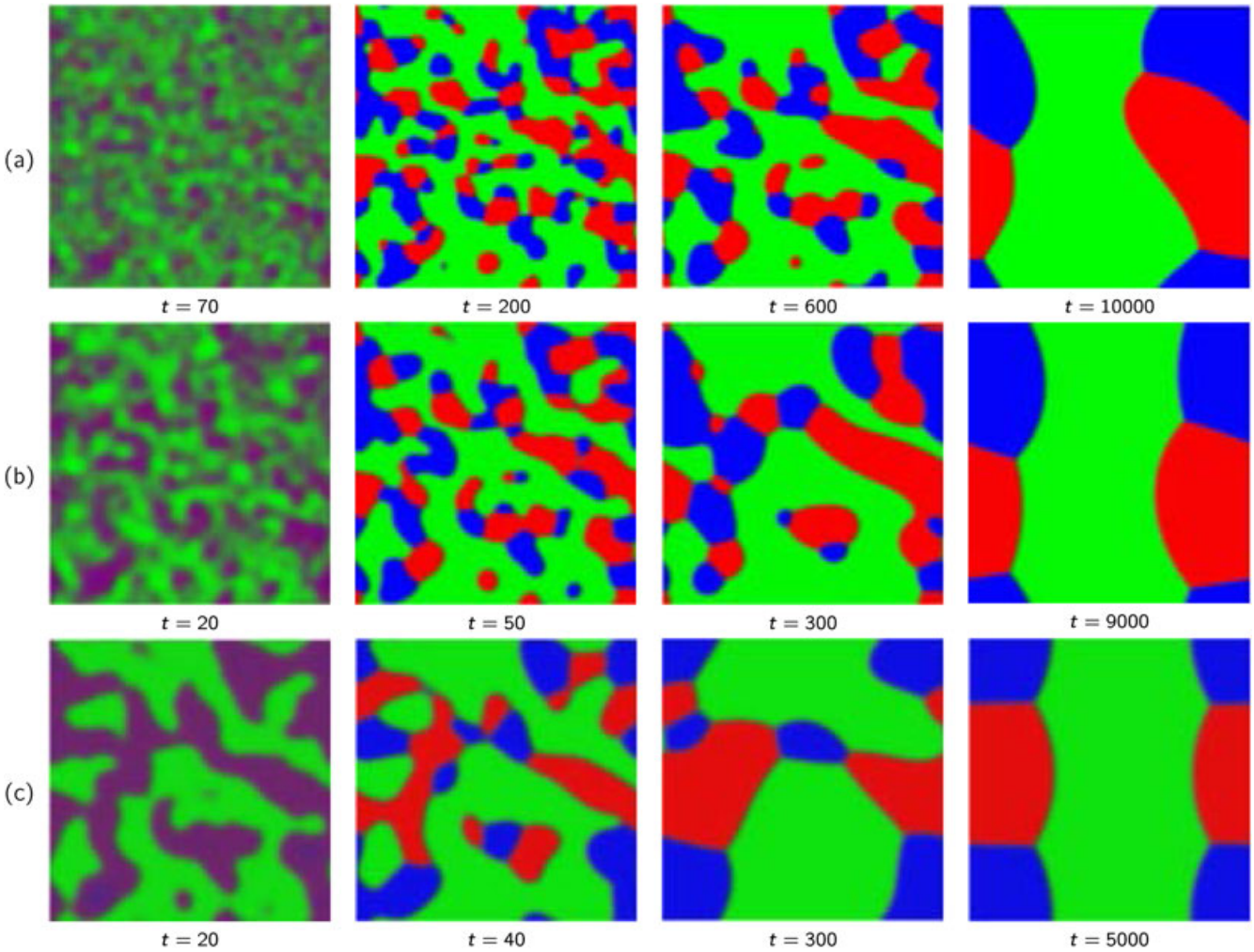

Figure 9. Numerical solution of a ternary system at each time with (a) $\theta = 0.15$, (b) $\theta = 0.225$, and (c) $\theta = 0.3$. The times are shown at the bottom of each figure. [Colour figure can be viewed at wileyonlinelibrary.com]

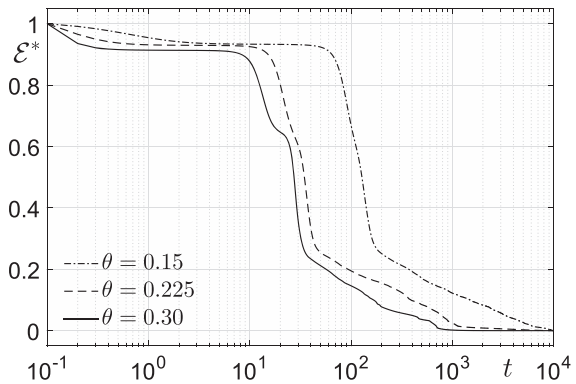

Figure 10. Scaled discrete energy of numerical solution on a ternary system with $\theta = 0.15$, $\theta = 0.225$, and $\theta = 0.3$.

where $|\alpha_k(t)|, |\beta_k(t)| \ll 1$ [17]. After linearizing the nonlinear terms in Eqs (1)–(4) about $(m, m, 1-2m)$, we have

$$\frac{\partial \phi}{\partial t} = \Delta \mu, \tag{24}$$

$$\begin{aligned} \mu = {} & \theta \ln(m) + \frac{\theta(\phi - m)}{m} - \theta_c \phi - \epsilon^2 \Delta \phi \\ & - \frac{\theta}{3}\left(\ln[m^2(1-2m)] + \frac{(1-3m)(\phi - m)}{m(1-2m)} + \frac{(1-3m)(\psi - m)}{m(1-2m)} \right), \end{aligned} \tag{25}$$

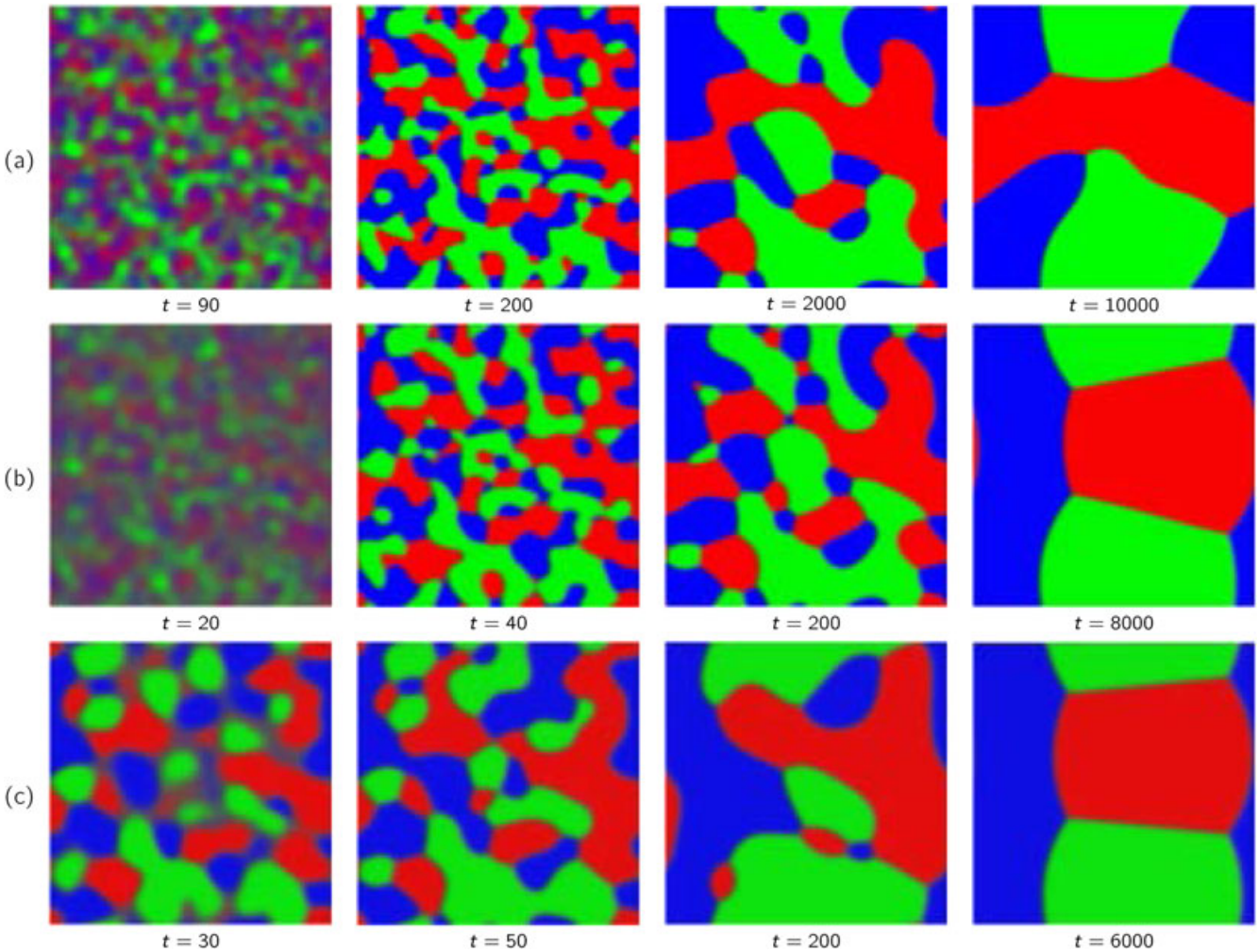

Figure 11. Numerical solution of a ternary system at each time with $\theta = 0.15$, 0.225, and 0.3. The times are shown at the bottom of each figure. [Colour figure can be viewed at wileyonlinelibrary.com]

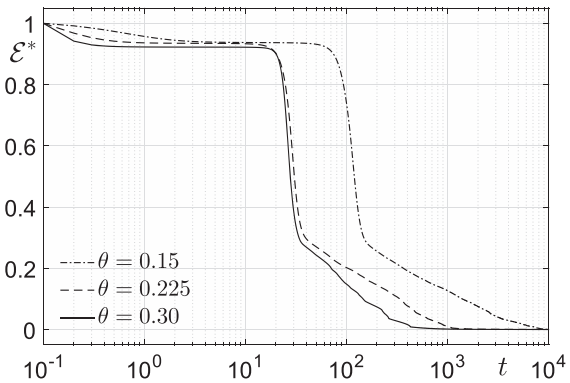

Figure 12. Scaled discrete energy of numerical solution on a ternary system with $\theta = 0.15$, 0.225, and 0.3.

$$\frac{\partial \psi}{\partial t} = \Delta \nu, \tag{26}$$

$$\begin{aligned} \nu = {} & \theta \ln(m) + \frac{\theta(\psi - m)}{m} - \theta_c \psi - \epsilon^2 \Delta \psi \\ & - \frac{\theta}{3}\left(\ln[m^2(1-2m)] + \frac{(1-3m)(\phi - m)}{m(1-2m)} + \frac{(1-3m)(\psi - m)}{m(1-2m)}\right). \end{aligned} \tag{27}$$

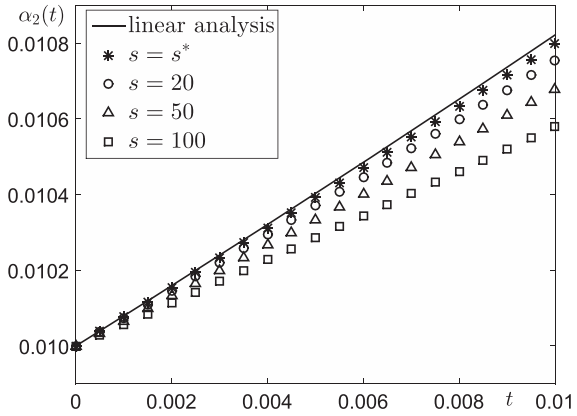

Figure 13. Temporal evolution of the numerical amplitude $\alpha_2(t)$ with different splitting factor s and its corresponding result by linear stability analysis.

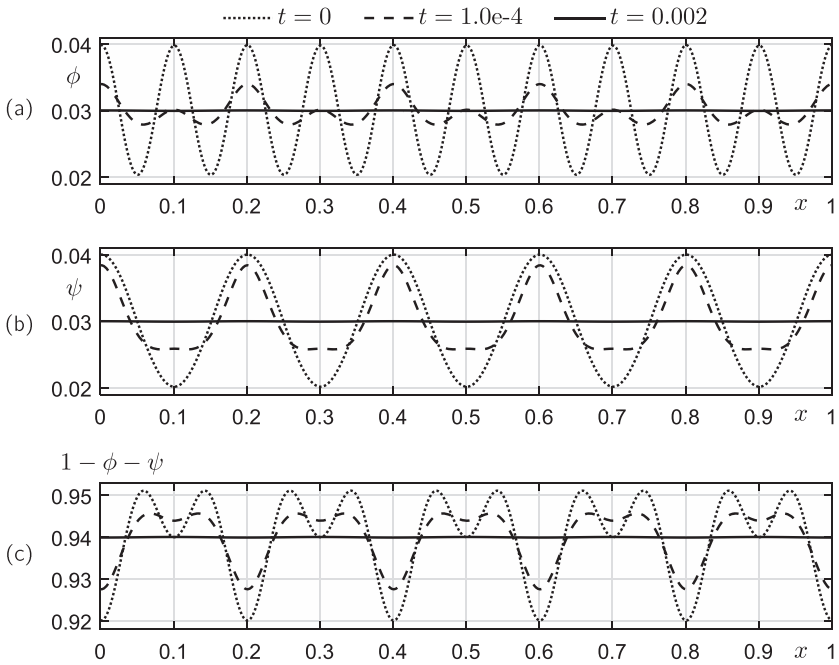

Figure 14. Phase transformation of (a) ϕ, (b) ψ, and (c) $1 - \phi - \psi$ in metastable region.

By substituting Eq. (23) into Eqs (24)–(27), we obtain

$$\begin{pmatrix} \alpha_k'(t) \\ \beta_k'(t) \end{pmatrix} = \mathbf{A} \begin{pmatrix} \alpha_k(t) \\ \beta_k(t) \end{pmatrix}, \quad \text{where } \mathbf{A} = \begin{pmatrix} a & b \\ b & a \end{pmatrix}, \tag{28}$$

$$\text{and } a = -(k\pi)^2 \left[\frac{\theta(2-3m)}{3m(1-2m)} - \theta_c + \epsilon^2 (k\pi)^2 \right], \; b = \frac{(k\pi)^2 \theta (1-3m)}{3m(1-2m)}.$$

The eigenvalues of $\mathbf{A}$ are $\lambda_1 = a - b$ and $\lambda_2 = a + b$. The solution to the system of the ordinary differential equations (28) is given by

$$\begin{pmatrix} \alpha_k(t) \\ \beta_k(t) \end{pmatrix} = \frac{e^{\lambda_1 t}}{2} \begin{pmatrix} -\alpha_k(0) + \beta_k(0) \\ \alpha_k(0) - \beta_k(0) \end{pmatrix} + \frac{e^{\lambda_2 t}}{2} \begin{pmatrix} \alpha_k(0) + \beta_k(0) \\ \alpha_k(0) + \beta_k(0) \end{pmatrix}.$$

For the numerical test, we take the initial condition as

$$\phi(x,0) = m + 0.01\cos(k\pi x), \; \psi(x,0) = m + 0.01\cos(k\pi x) \text{ on } \Omega = (0,1).$$

The other parameters are $m = 0.25$, $k = 2$, $h = 1/1000$, $\epsilon = h$, $\theta = 0.3$, $\theta_c = 1.0$, and its corresponding optimal splitting factor $s^* \approx 4.9972$. The numerical simulations are run up to $T = n\Delta t = 0.01$ with $\Delta t = 0.0001$. Figure 13 shows the temporal evolution of the numerical amplitudes $\alpha_k(t)$ and its corresponding linear stability analysis results. When $s = s^*$, the results are in good agreement in a linear regime. Also, through this test, we can see the dependence of the numerical solutions on the splitting factor s. As s is larger,

the numerical solution has smaller growth rate than the linear analysis. In other words, the larger splitting parameter s makes slow time evolution for numerical solution by generating a larger local truncation error. Therefore, we can confirm that s^* is an optimal splitting parameter.

3.4. *Phase transformation in metastable region*

As the last test, we consider phase transformation in metastable region, that is, $\phi(x,0) < \phi_{\min}$. Let the initial condition be given as $\phi(x,0) = 0.03 + 0.01\cos(20\pi x)$ and $\psi(x,0) = 0.03 + 0.01\cos(10\pi x)$ on the one-dimensional space $\Omega = [0,1]$. The other parameters are $N_x = 1000$, $h = 1.0\text{e-}3$, $\Delta t = 1.0\text{e-}6$, $T = 0.002$, $\epsilon = h$, $\theta = 0.3$, and $\theta_c = 1$. Figure 14(a)–(c) represents the temporal evolution for ϕ, ψ, and $1-\phi-\psi$, respectively. Because the initial condition is set in metastable region, we obtain the stable solution against initial perturbations as time goes on. Therefore, we can check that our algorithm works fine in the region a little away from $\phi_{\min}$.

4. Conclusions

In this paper, we proposed a practical estimation of a splitting parameter for a spectral method for the ternary CH system with a logarithmic free energy. By Eyre's convex splitting scheme, we derived a useful formula for the practical estimation of the splitting parameter in terms of the absolute temperature. In the previous research, finding an optimal splitting parameter has been carried out by trial and error. However, in this study, we can choose automatically an optimal splitting parameter by the derived formula. The numerical tests such as phase separation and total energy that decrease with different temperature values demonstrated that the proposed splitting parameter estimation gives stable numerical results. The linear stability test showed that the numerical solution with optimal value s has a good agreement with exact solution.

Appendix A. MATLAB code

The below MATLAB script is composed of 19 lines that are divided into two parts: (i) root-finding of equation (18) with **fzero** command and (ii) approximating a sixth-order best-fitted polynomial of the given data with **polyfit** command in MATLAB [15].

```
clear all; theta_c=1; n=41; theta=linspace(0.15,0.35,n);
gprime=@(x,t) 2*t*log(x/(1-2*x))+theta_c*(2-6*x)
for k=1:n
   fuc=@(x) gprime(x,theta(k));
   flag=1; iniguess=0.1;
   while flag==1
       phimin(k)=fzero(fuc,iniguess);
       if (phimin(k)>0 || phimin(k)<0)
           flag=0;
       else
           iniguess=iniguess/10;
       end
   end
end
p = polyfit(theta,phimin,6);
x1 = linspace(theta(1),theta(end),200); y1 = polyval(p,x1);
plot(theta,phimin,'ko'); hold on
plot(x1,y1,'k-'); axis([theta(1) theta(n) 0 max(phimin)])
legend('data','polynomial fit','Location','northwest)'
```

Acknowledgements

The first author (D. Jeong) was supported by a Korea University grant. The corresponding author (J.S. Kim) was supported by the National Research Foundation of Korea (NRF) grant funded by the Korea government (MSIP) (NRF-2014R1A2A2A01003683). The authors greatly appreciate the reviewers for their constructive comments and suggestions, which have improved the quality of this paper.

References

1. Copetti MIM. Numerical experiments of phase separation in ternary mixtures. *Mathematics and Computers in Simulation* 2000; **52**(1):41–51.
2. Garcke H, Nestler B, Stoth B. On anisotropic order parameter models for multi-phase systems and their sharp interface limits. *Physica D: Nonlinear Phenomena* 1998; **115**(1):87–108.
3. Cahn JW. On spinodal decomposition. *Acta Metallurgica* 1961; **9**(9):795–801.

4. Fontaine DD. *A computer simulation of the evolution of coherent composition variations in solid solutions*, Doctoral dissertation. Evanston IL: Northwestern University, 1967.
5. Fontaine DD. An analysis of clustering and ordering in multicomponent solid solutions–I Stability criteria. *Journal of Physics and Chemistry of Solids* 1972; **33**(2):297–310.
6. Fontaine DD. An analysis of clustering and ordering in multicomponent solid solutions–II fluctuations and kinetics. *Journal of Physics and Chemistry of Solids* 1973; **34**(8):1285–1304.
7. Morral JE, Cahn JW. Spinodal decomposition in ternary systems. *Acta Metallurgica* 1971; **19**(10):1037–1045.
8. Honjo M, Saito Y. Numerical simulation of phase separation in Fe–Cr binary and Fe–Cr–Mo ternary alloys with use of the Cahn–Hilliard equation. *ISIJ International* 2000; **40**(9):914–919.
9. Suwa Y, Saito Y, Ochi K, Aoki T, Goto K, Abe K. Kinetics of phase separation in Fe–Cr–Mo ternary alloys. *Materials Transactions* 2002; **43**(2):271–276.
10. Wang T, Sheng G, Liu ZK, Chen LQ. Coarsening kinetics of γ' precipitates in the Ni–Al–Mo system. *Acta Materialia* 2008; **56**(19):5544–5551.
11. Miyazaki T, Koyama T, Kozakai T. Computer simulations of the phase transformation in real alloy systems based on the phase field method. *Materials Science and Engineering: A* 2001; **312**(1):38–49.
12. Avila-Davila EO, Melo-Maximo DV, Lopez-Hirata VM, Soriano-Vargas O, Saucedo-Munoz ML, Gonzalez-Velazquez JL. Microstructural simulation in spinodally-decomposed Cu–70 at.% Ni and Cu–46 at % Ni–4 at % Fe alloys. *Materials Characterization* 2009; **60**(6):560–567.
13. Eyre DJ. Unconditionally gradient stable time marching the Cahn–Hilliard equation. In *MRS Proceedings*, Vol. 529. Cambridge University Press: Warrendale PA, 1998.
14. Eyre DJ. Systems of Cahn–Hilliard equations. *SIAM Journal on Applied Mathematics* 1993; **53**(6):1686–1712.
15. *MATLAB and Statistics Toolbox Release 2014b*. The MathWorks, Inc.: Natick, Massachusetts, United States.
16. Tavakoli R. Unconditionally energy stable time stepping scheme for Cahn–Morral equation: application to multi-component spinodal decomposition and optimal space tiling. *Journal of Computational Physics* 2016; **304**:441–464.
17. Blowey JF, Copetti MIM, Elliott CM. Numerical analysis of a model for phase separation of a multicomponent alloy. *IMA Journal of Numerical Analysis* 1996; **16**(1):111–139.